Topological field-effect transistor with quantized ON/OFF conductance of helical/chiral dislocation states

Xiaoyin Li and Feng Liu*
Department of Materials Science and Engineering, University of Utah, Salt Lake City, Utah 84112, USA

(Received 7 November 2022; accepted 23 May 2023; published 5 June 2023)

Topology is a key ingredient driving the emergence of quantum devices. The topological field-effect transistor (TFET) has been proposed to outperform the conventional field-effect transistor by replacing the ON state with topology-protected quantized conductance, while the OFF state has the same normal insulating characteristics and hence bears similar drawbacks. Here, we demonstrate a proof-of-concept TFET, having both ON and OFF quantized conductance, by switching between helical and chiral topological screw dislocation (SD) states in three-dimensional topological insulators. A pair of SDs are configured, with one acting as a channel and the other as a gate controlled by a local magnetic field. Reversible field switching is achieved with the ON and OFF conductance of $2e^2/h$ and e^2/h, respectively, as shown by tight-binding quantum transport calculations. Furthermore, $BaBiO_3$ is shown as one candidate material that has the desired topological SD states, based on first-principles calculations. Our findings open a new route to high-fidelity topological quantum devices.

DOI: 10.1103/PhysRevB.107.224101

I. INTRODUCTION

Topology and quantum coherence are two key ingredients driving the emergence of quantum devices with superior functionalities over conventional electronic devices. Topological materials featured with topology-protected quantum states are perfect candidates to improve device performance through quantized coherent charge and spin transport with minimized heat dissipation and robustness against disorder scattering [1–3]. Since the first proposals of quantum spin Hall insulators (QSHIs) [4,5], extensive theoretical and experimental efforts have been made to uncover high-quality topological materials [6–19] and disclose conceptually new quantum devices to take full advantage of topological properties [20,21].

The field-effect transistor (FET) is a basic building block of modern electronic devices, and operates by switching the electric signals between high and low conductivities, known as the ON and OFF states. Robust and precise ON and OFF signals and a high ON/OFF ratio are essential for high-performance FETs. Conventional FETs based on semiconductors usually experience multiple scatterings in transport of charge carriers, causing dissipation of energy and generation of waste heat, limiting device performance. To overcome such constraints, topological field-effect transistors (TFETs) utilizing topological surface or edge states as conducting channels, which are immune to external perturbations and nonmagnetic disorders, have been proposed as an improvement over conventional counterparts [1,2,22,23]. To date, however, the reported TFETs generally exploit a topological metallic state and a trivial insulating state, with the former functioning as the ON state and the latter as the OFF state [24–30]. Consequently, although the ON state of such TFETs has topological quantized conductance, the OFF state of a normal insulator experiences similar drawbacks as conventional FETs, especially the disorder-induced current leakage [31], resulting in a nonzero OFF signal and a decreased ON/OFF ratio.

It is important to recognize that the reason for a finite ON/OFF ratio for conventional FET is the leakage current in the OFF state—namely, the OFF state does not have an exact zero current. This is even true for all the previously proposed TFETs. To overcome this outstanding problem, one must find a *physical mechanism* to eliminate the leakage current, which is what we have objectively achieved in this work. In this Letter, we exploit the potential of topological dislocation states in three-dimensional (3D) topological insulators (TIs), and propose a conceptually new high-fidelity TFET with both quantized ON and OFF states.

Dislocations are commonly seen in crystalline materials as line defects [32–34], which are usually thought to be detrimental to material properties [35–38]. However, recent studies have demonstrated the prospect of reinventing dislocations as a valuable resource, such as for spintronics applications [39,40]. Interestingly, dislocations in 3D TIs have been demonstrated to induce topological gapless states when their Burgers vector **b** and the bulk topological invariants satisfy certain rules [41,42]. Taking advantage of this existing knowledge, we demonstrate that a pair of screw dislocations (SDs) in 3D TIs can serve as one-dimensional (1D) conducting channels harvesting helical topological gapless states lying in the bulk bandgap, contributing a quantized conductance of $2e^2/h$. Moreover, one of the two pairs of conducting channels can be selectively gapped out by applying a local Zeeman field, with the other pair left intact, contributing a quantized conductance of e^2/h associated with the 1D chiral topological line states. Accordingly, we devise a proof-of-concept TFET as illustrated in Fig. 1, where a pair of SDs are configured with one acting as a channel contacted with two metal leads and the

*Corresponding author: fliu@eng.utah.edu

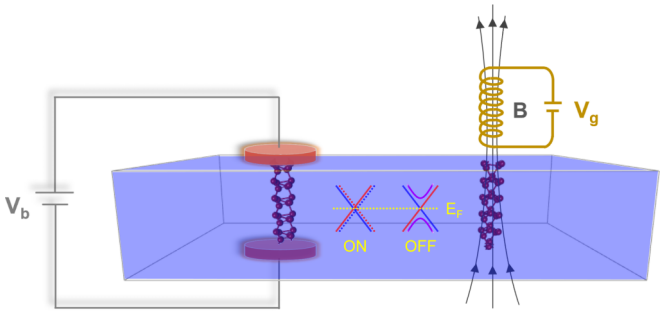

FIG. 1. Schematic illustration of the high-fidelity TFET enabled by topological dislocation states. The local leads, with a bias voltage V_b, cover one dislocation, acting as a quantized conducting channel. The magnetic field generated by the gate voltage V_g is applied to the other dislocation, acting as a gate to switch between the quantized ON and OFF states. The inset displays the metallic helical/chiral states for the ON/OFF operation. E_F is the Fermi level.

other as a gate controlled by a local magnetic field generated by a gate voltage. The conducting channels of topological dislocation states are reversibly switched between helical and chiral states by the local magnetic field, constituting the ON and OFF states with a quantized conductance of $2e^2/h$ and e^2/h, respectively. As the ON and OFF states are both topologically protected, the device is robust against disorders in the whole operation regime, as demonstrated directly by tight-binding (TB) quantum transport calculations.

By designing the OFF state to operate in a topologically protected regime with a quantized conductivity $1 \cdot (e^2/h)$, it will be as robust as the ON state operating with a quantized conductivity $2 \cdot (e^2/h)$. So, physically the theoretical limit of the ON/OFF ratio is infinite without the leakage current in the OFF state, or numerically one can use e^2/h (fundamental constants) as a reference of "zero" conductance, so that the ON/OFF ratio can be calculated as $(2-1)/(1-1) = \infty$ by converting "1" into an exact "0" via signal processing, since the OFF-state conductance can never be deviated from one. Furthermore, as a major step toward practical applications, we propose a strong 3D TI, $BaBiO_3$ [43], as one of candidate materials to realize the desired tunable topological dislocation states.

II. MODEL

To illustrate the key principle of our proposal, the Fu-Kane-Mele model on a diamond lattice [44] hosting SDs is adopted for illustration. The TB Hamiltonian based on a single-orbital diamond lattice reads [44,45]

$$H = t \sum_{\langle ij \rangle} c_i^\dagger c_j + i\lambda_{\mathrm{SO}} \sum_{\langle\langle ij \rangle\rangle} c_i^\dagger \boldsymbol{s} \cdot \hat{\boldsymbol{e}}_{ij} c_j. \tag{1}$$

The first term corresponds to nearest-neighbor (NN) hopping and the second term to second NN spin-orbit coupling (SOC), with $c^\dagger$ (c) being the electron creation (annihilation) operator. $\mathbf{s}$ denotes the vector of spin Pauli matrices and $\hat{\boldsymbol{e}}_{ij}$ is the unit vector defined by $\hat{\boldsymbol{e}}_{ij} = (\vec{d}_{ij}^{\,1} \times \vec{d}_{ij}^{\,2})/|\vec{d}_{ij}^{\,1} \times \vec{d}_{ij}^{\,2}|$, where $\vec{d}_{ij}^{\,1}$ and $\vec{d}_{ij}^{\,2}$ are the two NN bond vectors connecting the second NN orbitals j and i. We set $t = -1$ and $\lambda_{\mathrm{SO}} = -0.3$, and

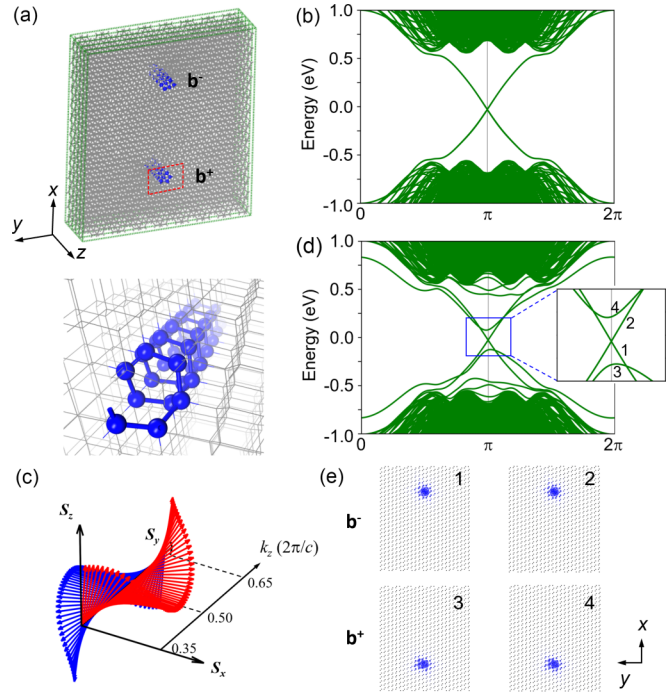

FIG. 2. (a) Top panel: A pair of separated SDs in a diamond lattice. The green dashed lines indicate the supercell containing 1248 single orbital sites, within which a pair of SDs having opposite Burgers vectors ($\mathbf{b}^+/\mathbf{b}^-$) are created, and the dislocation cores are highlighted in blue. The red rectangle marks the region where the local field is applied. Bottom panel: Perspective view of one SD. (b) Energy bands of the dislocated supercell showing SD-induced topological gapless states. (c) Spin textures of a pair of topological SD states. (d) Energy bands in the presence of a local field at one SD. The inset shows the zoomed-in bands near the band crossing point. (e) Charge density distributions of the four bands indicated in (d), localized around the $\mathbf{b}^+/\mathbf{b}^-$ SD core. The k path for energy bands is along the SD core direction.

the NN hopping along the [111] direction is intentionally enhanced to $(t + \delta t)$, with $\delta t = -1$, to drive the model into a strong TI phase having topological indices (1;111) [44]. All parameters are in the unit of electron volts. As shown previously [41], the dislocation will induce topological gapless states if its Burgers vector $\mathbf{b}$ and the time-reversal invariant momentum (TRIM) $\mathbf{M}_\nu$ of the bulk material satisfy

$$\mathbf{b} \cdot \mathbf{M}_\nu = \pi \,(\mathrm{mod}\, 2\pi). \tag{2}$$

The TRIM is defined by $\mathbf{M}_\nu = (1/2)(\nu_1\mathbf{G}_1 + \nu_2\mathbf{G}_2 + \nu_3\mathbf{G}_3)$, where (ν_1, ν_2, ν_3) and $(\mathbf{G}_1, \mathbf{G}_2, \mathbf{G}_3)$ are the weak topological indices and the reciprocal lattice vectors, respectively. Given the lattice vectors $(\mathbf{a}_1, \mathbf{a}_2, \mathbf{a}_3)$, we introduce a pair of separated SDs with the opposite Burgers vectors $\mathbf{b} = \pm\mathbf{a}_3$ to restore the periodic boundary condition yielding $\mathbf{b} \cdot \mathbf{M}_\nu = \pm\pi$. We note that our proposal is not constrained to the paired SDs, but also works when the supercell contains a single SD, as demonstrated in Supplemental Material Sec. VII [46].

Figure 2(a) shows the geometric structure of the considered SDs, whose core extends along the z direction. The calculated band structures in Fig. 2(b) demonstrate the emergence of

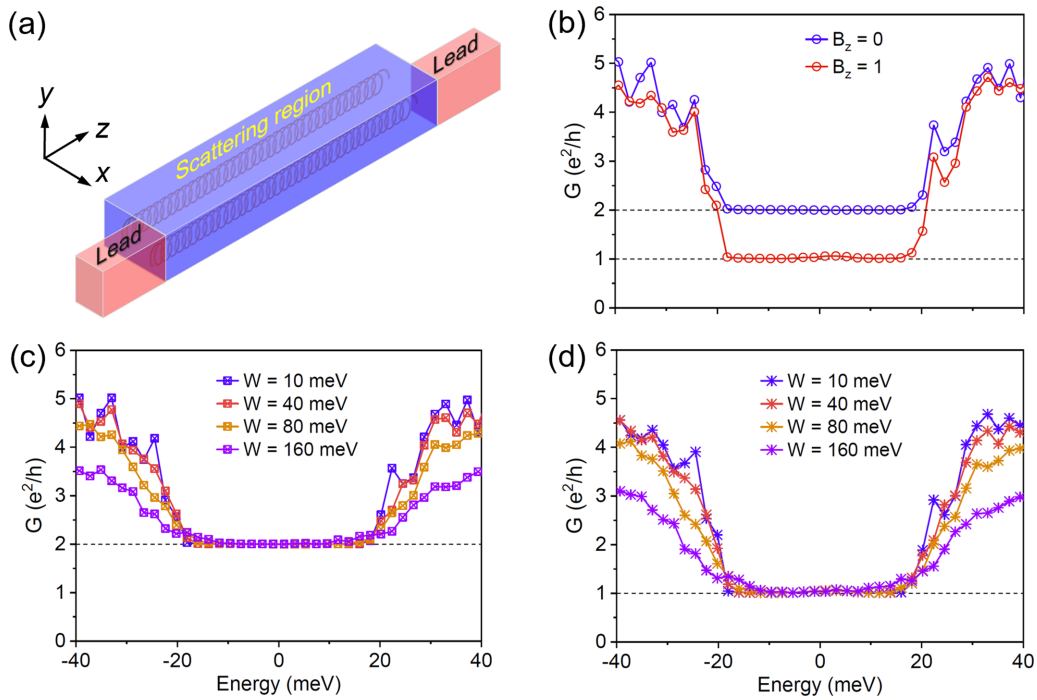

FIG. 3. (a) A schematic view of the device setup to conduct transport simulations. The size of the scattering region is $1 \times 1 \times 80$ times the periodic supercell. The leads cover half of the scattering region and one SD, while the local field is applied on the other SD. (b) Conductance as a function of energy in the absence and presence of the local Zeeman field. (c) and (d) Conductance results against disorders for $B_z = 0$ and 1, respectively. W indicates the strength of the disorder. For a specific disorder strength, the conductance is averaged over 50 different disorder configurations, which is sufficient to obtain the converged results.

topological gapless states within the bulk bandgap, consistent with the criterion of Eq. (2) [41]. Like the helical topological edge states of QSHIs, the topological SD states contain four (two pairs) 1D modes. They are highly localized at the dislocation cores, and each pair carries oppositely propagating gapless states. In Fig. 2(c), we present the spin textures of one pair of helical modes localized at one SD, showing that the spin polarization whirls along the k path. Consequently, one can effectively manipulate the spin polarization direction of the topological SD states by tuning the Fermi energy, which provides an additional degree of freedom for spintronics applications [54–56]. We also found that the distortion strength δt is the key factor to change the period of spin polarization evolution (see Supplemental Material Fig. S1 [46]), implying that the detailed spin texture is dependent of the structural symmetry, which affords the possibility of delicate manipulation via strain engineering [57].

We then explore the possibility of tuning the topological SD states by a local Zeeman field, e.g., by applying a magnetic field or proximity to a magnetic material, which has been demonstrated to tailor the topological states efficiently [58–60]. Its effect can be included in the TB model by adding the term $H_B = \sum_{i \in Z_B} c_i^\dagger \boldsymbol{B} \cdot \boldsymbol{s} c_i$. Here, Z_B indicates a local region where the Zeeman field is applied, as illustrated by the red rectangle in Fig. 2(a). Figure 2(d) shows the band structures for $B_z = 1$. Upon a finite z-direction Zeeman field, the Kramers degeneracy of one pair of SD states is lifted, opening a gap between two topological SD states while the other two remain gapless. By analyzing the charge density distributions of the four states as displayed in Fig. 2(e), we identify that the gapped states are located around the SD covered by the local Zeeman field, as expected, whereas the gapless states around the other SD remain intact away from the Zeeman field, whose spin textures are also checked and remain the same. These results indicate that the local Zeeman field can selectively remove one pair of topological SD states. In other words, the local Zeeman field breaks the time-reversal symmetry to destroy the topological helical states, driving the system into a different topological phase displaying topological chiral states. This essentially realizes a field-controlled switching between topological helical and chiral states. The detailed mechanism of gap opening in relation to spin orientation by a Zeeman field, and energy band evolution under different strengths of a Zeeman field can be found in Supplemental Material Sec. III [46]. It is worth noting that, similar to the proposed selectively gapping of topological SD states, experiments have confirmed the feasibility of gapping out only one surface state of 3D TIs by magnetic doping while keeping the other surface state on the opposite side intact [61,62].

III. ROBUST QUANTIZED TRANSPORT OF TOPOLOGICAL SD STATES

Based on the previous insights from TB modeling, we next study the quantum transport property of the topological SD states and the tunability by a local Zeeman field using a two-terminal mesoscopic setup as shown in Fig. 3(a). The scattering region is a finite system built by the supercell of Fig. 2(a) containing a pair of SDs, while two semi-infinite metallic leads are attached along one SD core, the channel,

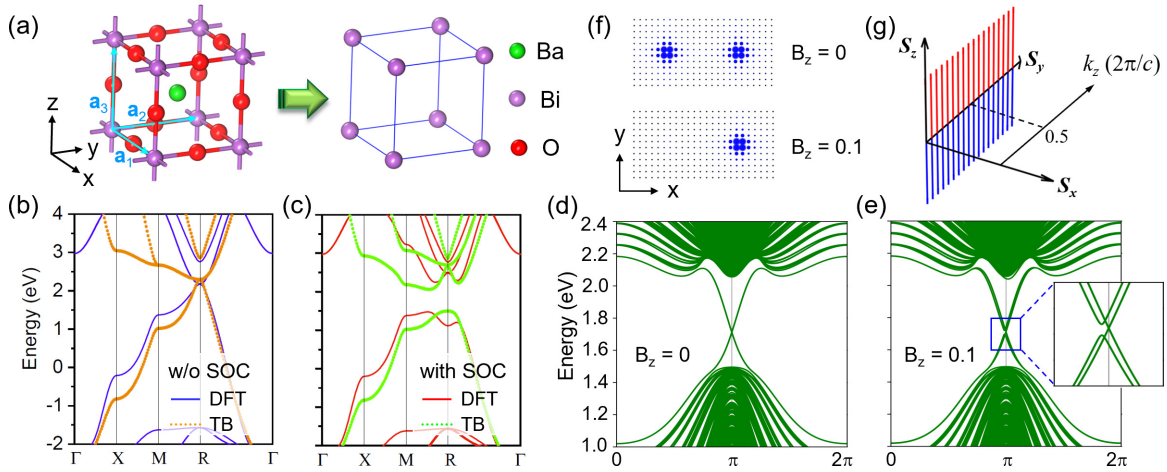

FIG. 4. (a) Atomic structure of cubic $BaBiO_3$ and its bismuth sublattice. (b) and (c) Energy bands of $BaBiO_3$ without and with SOC, respectively. (d) and (e) Energy bands of the dislocated supercell in the absence and presence of the local field, respectively. The k path is along the SD core direction. (f) Charge density distributions of the topological gapless states. Here, only a portion of the structure around the SDs is shown. (g) Spin textures of the preserved gapless states for $B_z = 0.1$ eV.

to provide transport carriers (as shown in Fig. 1). The Kwant software package [63] is employed to build the device and numerically solve the transport problem within the Landauer-Buttiker formalism [64]. Figure 3(b) displays the calculated conductance as a function of energy in the absence and presence of the local Zeeman field at the other SD, the gate. The quantized plateaus are observed for both cases, sitting at $2e^2/h$ and e^2/h, respectively, consistent with the number of quantized transmission channels for the 1D topological helical and chiral states. Here, the conductance plateau only exists in an energy range of ~ 40 meV, much smaller than the large nontrivial bandgap, as shown in Fig. 2(b). This is caused by the finite size of the scattering region in the transverse directions, which gives rise to surface states that drastically reduce the band gap (see Supplemental Material Sec. IV [46] for details).

We further check the robustness of the topological SD states against disorder. The Anderson-type onsite disorder is introduced by adding a term $W\sum_i \xi_i c_i^\dagger c_i$ to the TB model in the scattering region. ξ_i is a random variable uniformly distributed in the interval of [–1, 1], and W represents the strength of disorder. Figure 3(c) shows the calculated conductance results of the pristine topological SD states under different disorder strengths. One can see that, although the conductance drops with increasing disorder strength for energies outside the nontrivial bandgap, the conductance plateau of $2e^2/h$ is preserved up to $W = 160$ meV, confirming the topological protection and robustness of the SD gapless states. Figure 3(d) shows the results when the local Zeeman field is applied. The conductance plateau quantized at e^2/h persists for all considered disorder strengths, further confirming that the gapless states are topologically protected even in the presence of a local Zeeman field. Our transport calculations demonstrate convincingly that the conductance of the topological SD states can be switched from one quantized value ($2e^2/h$) to another (e^2/h) using the local Zeeman field as a knob. This finding is very inspiring for disclosing a new recipe to realize two topologically protected conductance signals in a single material, which renders our proposed TFETs with unprecedented high robustness and precision.

IV. MATERIAL CANDIDATES

Before closing, possible materials hosting the predicted tunable topological SD states are explored. Considering the diamond lattice we used for the model study, bulk Bi holding a similar crystal structure naturally comes to our mind [65]. However, the pristine bulk bismuth is a higher order TI with topological indices (0;000) [66], which cannot give topological dislocation states according to Eq. (2). Although it can be tuned into a strong TI phase by strain, the bulk bands will overwhelm the topological SD states due to the nonglobal, narrow bandgap [67]. To obtain clean topological SD states separated from bulk states, we first switch attention to a large energy gap oxide TI, $BaBiO_3$, with a cubic perovskite structure [Fig. 4(a)] [43]. $BaBiO_3$ has the topological indices (1;111) and a large nontrivial gap in the conduction bands. Since the topologically relevant band inversion only involves Bi-6s and Bi-6p orbitals [43], one can adopt a simplified model with the basis of Bi-(s, p_x, p_y, p_z) to capture the essential low-energy physics around its nontrivial band gap (see Supplemental Material Sec. VIII [46] for details). Figure 4(b) and 4(c) shows the corresponding band structures, with good consistence between TB model and density functional theory calculation. Accordingly, the $BaBiO_3$ structure is reduced to a bismuth sublattice, as shown in Fig. 4(a). By introducing a pair of SDs to a supercell of the representative bismuth sublattice, whose Burgers vectors are $\mathbf{b}= \pm\mathbf{a}_3$ satisfying Eq. (2) (see Supplemental Material Fig. S11 [46]), we obtain the band structure in Fig. 4(d), exhibiting a pair of topological SD states inside the bulk gap. We also checked the band structure of the same supercell without SDs to ensure it does not have gapless states (see Supplemental Material Fig. S12 [46]).

Next, we investigate the field tunability of these gapless states by applying a local Zeeman field B_z covering one of the two SDs. Figure 4(e) shows that a pair of SD bands

open a gap of ∼20 meV, while the other pair remains gapless for $B_z = 0.1$ eV. Figure 4(f) displays the corresponding charge density distributions, confirming again that the local field selectively removes one pair of SD states. Also, the spin textures of the preserved gapless states are shown in Fig. 4(g), which remain intact with the local field. Here, the spin textures have small y components (see Supplemental Material Fig. S13 [46]), perpendicular to the Zeeman field (B_z), resulting in the bandgap opening. All these results agree with our Fu-Kane-Mele TB model studies, suggesting $BaBiO_3$ as a potential material candidate to achieve the desired topological SD states. Considering that topological materials with strong SOC can have very large, effective g factors [68], the proposed Zeeman field can be achievable through a feasible magnetic field (see Supplemental Material Fig. S14 [46]). Besides $BaBiO_3$, another promising candidate is $GeBi_2Te_4$ with topological indices (1;111) (see Supplemental Material Sec. XI for related discussions [46]). It is worth mentioning that the controllable formation of screw dislocations can be realized in experiments via epitaxial growth of thin films on substrates [39,69] or wafer bonding processes [70–72].

V. CONCLUSIONS

The concept of high-fidelity TFETs operating with both ON and OFF states of quantized conductance as we demonstrated is general. It significantly broadens the functionalities of TIs for quantum device applications. The physical principle we disclose for implementing topological dislocation states in FETs may also be applied to edge states of 2D TIs or hinge states of 3D high-order TIs with a proper choice of field direction relative to spin textures. Compared with the edge/hinge states localized on the boundary and constituting an outer channel, the dislocations are usually located inside the bulk away from material boundaries, constituting an inner channel less sensitive to external noise and easier for device implementation. Moreover, multiple channels/gates may be fabricated in one material platform by generating dislocation arrays, which could be harder if using edges or hinges. To generalize the proposed mechanism of "fully topological" ON/OFF signals, we suggest that Chern number tunable quantum anomalous Hall insulators may also be used for realizing the proposed high-fidelity TFET. The Chern number characterizing the dissipationless chiral edge states can be tuned either by varying the composition of the multilayered materials [73–75] or by manipulating the magnetization orientation of specific materials [76], which endows the systems with different quantized conductance. In this context, a feasible "gate" to switch the system effectively between different Chern numbers can be further explored. As a final note, in proximity with a superconductor, our proposed Zeeman field-tuned topological dislocation states may offer a new platform for realizing Majorana zero mode at one or many dislocation cores to function as quantum bits.

ACKNOWLEDGMENTS

We thank X. M. Zhang for helpful discussions. We acknowledge the support of the US DOE-BES (Grant No. DE-FG02-04ER46148). Computational resources for this work were supported by CHPC of the University of Utah and the DOE-NERSC.

[1] M. Z. Hasan and C. L. Kane, Rev. Mod. Phys. **82**, 3045 (2010).
[2] X.-L. Qi and S.-C. Zhang, Rev. Mod. Phys. **83**, 1057 (2011).
[3] A. Bansil, H. Lin, and T. Das, Rev. Mod. Phys. **88**, 021004 (2016).
[4] C. L. Kane and E. J. Mele, Phys. Rev. Lett. **95**, 146802 (2005).
[5] C. L. Kane and E. J. Mele, Phys. Rev. Lett. **95**, 226801 (2005).
[6] B. A. Bernevig, T. L. Hughes, and S.-C. Zhang, Science **314**, 1757 (2006).
[7] M. König, S. Wiedmann, C. Brüne, A. Roth, H. Buhmann, L. W. Molenkamp, X.-L. Qi, and S.-C. Zhang, Science **318**, 766 (2007).
[8] H. Zhang, C.-X. Liu, X.-L. Qi, X. Dai, Z. Fang, and S.-C. Zhang, Nat. Phys. **5**, 438 (2009).
[9] Y. Xia, D. Qian, D. Hsieh, L. Wray, A. Pal, H. Lin, A. Bansil, D. Grauer, Y. S. Hor, R. J. Cava, and M. Z. Hasan, Nat. Phys. **5**, 398 (2009).
[10] D. Hsieh, Y. Xia, D. Qian, L. Wray, J. H. Dil, F. Meier, J. Osterwalder, L. Patthey, J. G. Checkelsky, N. P. Ong, A. V. Fedorov, H. Lin, A. Bansil, D. Grauer, Y. S. Hor, R. J. Cava, and M. Z. Hasan, Nature (London) **460**, 1101 (2009).
[11] Y. L. Chen, J. G. Analytis, J. H. Chu, Z. K. Liu, S. K. Mo, X. L. Qi, H. J. Zhang, D. H. Lu, X. Dai, Z. Fang, S. C. Zhang, I. R. Fisher, Z. Hussain, and Z. X. Shen, Science **325**, 178 (2009).
[12] C.-Z. Chang *et al.*, Science **340**, 167 (2013).
[13] Z. F. Wang, K.-H. Jin, and F. Liu, WIREs Comput. Mol. Sci **7**, e1304 (2017).
[14] M. G. Vergniory, L. Elcoro, C. Felser, N. Regnault, B. A. Bernevig, and Z. Wang, Nature (London) **566**, 480 (2019).
[15] F. Tang, H. C. Po, A. Vishwanath, and X. Wan, Nature (London) **566**, 486 (2019).
[16] T. Zhang, Y. Jiang, Z. Song, H. Huang, Y. He, Z. Fang, H. Weng, and C. Fang, Nature (London) **566**, 475 (2019).
[17] Y. Xu, L. Elcoro, Z.-D. Song, B. J. Wieder, M. G. Vergniory, N. Regnault, Y. Chen, C. Felser, and B. A. Bernevig, Nature (London) **586**, 702 (2020).
[18] R.-J. Slager, A. Mesaros, V. Juričić, and J. Zaanen, Nat. Phys. **9**, 98 (2013).
[19] J. Kruthoff, J. de Boer, J. van Wezel, C. L. Kane, and R.-J. Slager, Phys. Rev. X **7**, 041069 (2017).
[20] M. J. Gilbert, Commun. Phys. **4**, 70 (2021).
[21] M. S. Lodge, S. A. Yang, S. Mukherjee, and B. Weber, Adv. Mater. **33**, 2008029 (2021).
[22] M. König, H. Buhmann, L. W. Molenkamp, T. Hughes, C.-X. Liu, X.-L. Qi, and S.-C. Zhang, J. Phys. Soc. Jpn. **77**, 031007 (2008).
[23] C.-X. Liu, S.-C. Zhang, and X.-L. Qi, Annu. Rev. Condens. Matter Phys. **7**, 301 (2016).
[24] X. Qian, J. Liu, L. Fu, and J. Li, Science **346**, 1344 (2014).
[25] L. Fleet, Nat. Phys. **11**, 5 (2015).
[26] J. Liu, T. H. Hsieh, P. Wei, W. Duan, J. Moodera, and L. Fu, Nat. Mater. **13**, 178 (2014).

[27] J. L. Collins, A. Tadich, W. Wu, L. C. Gomes, J. N. B. Rodrigues, C. Liu, J. Hellerstedt, H. Ryu, S. Tang, S.-K. Mo, S. Adam, S. A. Yang, M. S. Fuhrer, and M. T. Edmonds, Nature (London) **564**, 390 (2018).

[28] X. Li, F. Liu, and Q. Wang, Phys. Rev. B **102**, 195420 (2020).

[29] J. Chen, T. Zhang, J. Wang, L. Xu, Z. Lin, J. Liu, C. Wang, N. Zhang, S. P. Lau, W. Zhang, M. Chhowalla, and Y. Chai, Sci. Adv. **8**, eabn3837 (2022).

[30] M. Ezawa, Appl. Phys. Lett. **102**, 172103 (2013).

[31] Y. Zhang, M. Sun, H. Y. Wong, Y. Lin, P. Srivastava, C. Hatem, M. Azize, D. Piedra, L. Yu, T. Sumitomo, N. A. D. Braga, R. V. Mickevicius, and T. Palacios, IEEE Trans. Electron Devices **62**, 2155 (2015).

[32] D. Hull and D. J. Bacon, *Introduction to Dislocations*, 5th ed. (Butterworth-Heinemann, Oxford, 2011).

[33] P. M. Anderson, J. P. Hirth, and J. Lothe, *Theory of Dislocations* (Cambridge University Press, New York, 2017).

[34] R. M. Broudy, Adv. Phys. **12**, 135 (1963).

[35] F. M. Ross, R. Hull, D. Bahnck, J. C. Bean, L. J. Peticolas, and C. A. King, Appl. Phys. Lett. **62**, 1426 (1993).

[36] H. M. Ng, D. Doppalapudi, T. D. Moustakas, N. G. Weimann, and L. F. Eastman, Appl. Phys. Lett. **73**, 821 (1998).

[37] D. C. Look and J. R. Sizelove, Phys. Rev. Lett. **82**, 1237 (1999).

[38] L. M. Giovane, H.-C. Luan, A. M. Agarwal, and L. C. Kimerling, Appl. Phys. Lett. **78**, 541 (2001).

[39] L. Hu, H. Huang, Z. Wang, W. Jiang, X. Ni, Y. Zhou, V. Zielasek, M. G. Lagally, B. Huang, and F. Liu, Phys. Rev. Lett. **121**, 066401 (2018).

[40] X. Li, S. Zhang, H. Huang, L. Hu, F. Liu, and Q. Wang, Nano Lett. **19**, 6005 (2019).

[41] Y. Ran, Y. Zhang, and A. Vishwanath, Nat. Phys. **5**, 298 (2009).

[42] R.-J. Slager, A. Mesaros, V. Juričić, and J. Zaanen, Phys. Rev. B **90**, 241403(R) (2014).

[43] B. Yan, M. Jansen, and C. Felser, Nat. Phys. **9**, 709 (2013).

[44] L. Fu, C. L. Kane, and E. J. Mele, Phys. Rev. Lett. **98**, 106803 (2007).

[45] L. Fu and C. L. Kane, Phys. Rev. B **76**, 045302 (2007).

[46] See Supplemental Material at http://link.aps.org/supplemental/10.1103/PhysRevB.107.224101 for first-principles calculation methods, spin texture of topological SD states with varied model parameters, Zeeman-field tuned band gap in 1D dislocation line states, finite-size induced trivial surface states, energy bands evolution under different strength of Zeeman field, detailed results of SD states transport against disorders, supercell structure containing one SD, TB model and supplemental figures for the material candidate $BaBiO_3$, the minimum spatial distance between two SDs, and related discussions about the material candidate $GeBi_2Te_4$, which includes additional Refs. [47–53].

[47] G. Kresse and J. Furthmüller, Phys. Rev. B **54**, 11169 (1996).

[48] J. P. Perdew, K. Burke, and M. Ernzerhof, Phys. Rev. Lett. **77**, 3865 (1996).

[49] J. P. Perdew, K. Burke, and M. Ernzerhof, Phys. Rev. Lett. **78**, 1396(E) (1997).

[50] H. J. Monkhorst and J. D. Pack, Phys. Rev. B **13**, 5188 (1976).

[51] M. Neupane, S. Y. Xu, L. A. Wray, A. Petersen, R. Shankar, N. Alidoust, C. Liu, A. Fedorov, H. Ji, J. M. Allred, Y. S. Hor, T. R. Chang, H. T. Jeng, H. Lin, A. Bansil, R. J. Cava, and M. Z. Hasan, Phys. Rev. B **85**, 235406 (2012).

[52] M. M. Otrokov, T. V. Menshchikova, M. G. Vergniory, I. P. Rusinov, A. Y. Vyazovskaya, Y. M. Koroteev, G. Bihlmayer, A. Ernst, P. M. Echenique, A. Arnau, and E. V. Chulkov, 2D Mater. **4**, 025082 (2017).

[53] A. Zhuang, J.-J. Li, Y.-C. Wang, X. Wen, Y. Lin, B. Xiang, X. Wang, and J. Zeng, Angew. Chem. Int. Ed. **53**, 6425 (2014).

[54] R.-X. Zhang, H.-C. Hsu, and C.-X. Liu, Phys. Rev. B **93**, 235315 (2016).

[55] J. H. Garcia, M. Vila, C.-H. Hsu, X. Waintal, V. M. Pereira, and S. Roche, Phys. Rev. Lett. **125**, 256603 (2020).

[56] W. Zhao, E. Runburg, Z. Fei, J. Mutch, P. Malinowski, B. Sun, X. Huang, D. Pesin, Y.-T. Cui, X. Xu, J.-H. Chu, and D. H. Cobden, Phys. Rev. X **11**, 041034 (2021).

[57] C. Si, Z. Sun, and F. Liu, Nanoscale **8**, 3207 (2016).

[58] Y. Ren, Z. Qiao, and Q. Niu, Phys. Rev. Lett. **124**, 166804 (2020).

[59] R. Chen, T. Liu, C. M. Wang, H.-Z. Lu, and X. C. Xie, Phys. Rev. Lett. **127**, 066801 (2021).

[60] C. Wang, F. Liu, and H. Huang, Phys. Rev. Lett. **129**, 056403 (2022).

[61] R. Lu *et al.*, Phys. Rev. X **11**, 011039 (2021).

[62] M. Mogi, Y. Okamura, M. Kawamura, R. Yoshimi, K. Yasuda, A. Tsukazaki, K. S. Takahashi, T. Morimoto, N. Nagaosa, M. Kawasaki, Y. Takahashi, and Y. Tokura, Nat. Phys. **18**, 390 (2022).

[63] C. W. Groth, M. Wimmer, A. R. Akhmerov, and X. Waintal, New J. Phys. **16**, 063065 (2014).

[64] S. Datta, *Electronic Transport in Mesoscopic Systems* (Cambridge University Press, Cambridge, 1997).

[65] Z. Liu, C.-X. Liu, Y.-S. Wu, W.-H. Duan, F. Liu, and J. Wu, Phys. Rev. Lett. **107**, 136805 (2011).

[66] F. Schindler, Z. Wang, M. G. Vergniory, A. M. Cook, A. Murani, S. Sengupta, A. Y. Kasumov, R. Deblock, S. Jeon, I. Drozdov, H. Bouchiat, S. Guéron, A. Yazdani, B. A. Bernevig, and T. Neupert, Nat. Phys. **14**, 918 (2018).

[67] A. K. Nayak, J. Reiner, R. Queiroz, H. Fu, C. Shekhar, B. Yan, C. Felser, N. Avraham, and H. Beidenkopf, Sci. Adv. **5**, eaax6996 (2019).

[68] Z. Song, S. Sun, Y. Xu, S. Nie, H. Weng, Z. Fang, and X. Dai, in *Memorial Volume for Shoucheng Zhang* (World Scientific, Singapore, 2020).

[69] Y.-R. Chang, N. Higashitarumizu, H. Kawamoto, F.-H. Chu, C.-J. Lee, T. Nishimura, R. Xiang, W.-H. Chang, S. Maruyama, and K. Nagashio, Chem. Mater. **33**, 186 (2021).

[70] J. L. Rouviere, K. Rousseau, F. Fournel, and H. Moriceau, Appl. Phys. Lett. **77**, 1135 (2000).

[71] F. Fournel, H. Moriceau, B. Aspar, K. Rousseau, J. Eymery, J.-L. Rouvière, and N. Magnea, Appl. Phys. Lett. **80**, 793 (2002).

[72] X. Yu, T. Arguirov, M. Kittler, W. Seifert, M. Ratzke, and M. Reiche, Mater. Sci. Semicond. **9**, 96 (2006).

[73] H. Jiang, Z. Qiao, H. Liu, and Q. Niu, Phys. Rev. B **85**, 045445 (2012).

[74] J. Wang, B. Lian, H. Zhang, Y. Xu, and S.-C. Zhang, Phys. Rev. Lett. **111**, 136801 (2013).

[75] Y.-F. Zhao, R. Zhang, R. Mei, L.-J. Zhou, H. Yi, Y.-Q. Zhang, J. Yu, R. Xiao, K. Wang, N. Samarth, M. H. W. Chan, C.-X. Liu, and C.-Z. Chang, Nature (London) **588**, 419 (2020).

[76] Z. Li, Y. Han, and Z. Qiao, Phys. Rev. Lett. **129**, 036801 (2022).